Deformation Monitoring of Railway Bridges with a Profile Laser Scanner*

Florian Schill and Andreas Eichhorn

Summary

This paper presents the evaluation of the deformation monitoring of bridge structures with a profile scanner and shows that existing monitoring concepts can be extended with the use of profile scanning.

The contact-free acquisition method of a profile laser scanner reduces the expense for personnel and instrumentation compared to conventional sensors used for the monitoring of civil engineering structures. It furthermore enables the measurement of non-accessible areas of the monitored supporting structures. In addition, the availability of information along an entire structural profile can be used to flexibly deal with a wide variety of problems. With a measurement rate of at least 50 Hz, typical structural deformation signals can be recorded and sufficient data can be collected to characterize the underlying deformation processes dependably.

Zusammenfassung

Dieser Beitrag stellt die Überwachung von Brückentragwerken mit einem Profilscanner vor und zeigt, dass bestehende Konzepte klassischer Überwachungsmessungen mit Hilfe von Profilscannern ergänzt werden können.

Die berührungslose Erfassung mit einem Profilscanner reduziert den Aufwand für Personal und Instrumentierung im Vergleich zu herkömmlichen Sensoren, die zur Überwachung von Ingenieurbauwerken eingesetzt werden. Darüber hinaus wird die Messung von nicht zugänglichen Bereichen der überwachten Tragwerksstruktur ermöglicht. Zusätzlich kann die Verfügbarkeit von Informationen entlang eines gesamten Strukturprofils genutzt werden, um eine Vielzahl von Fragestellungen flexibel zu beantworten. Mit einer Messgeschwindigkeit von mindestens 50 Hz können so typische Verformungssignale der Struktur erfasst und ausreichend Daten erhoben werden, um die zugrunde liegenden Verformungsprozesse zuverlässig zu charakterisieren.

Keywords: deformation monitoring, profile laser scanning, supporting structures, bridges, spatio temporal processing scheme

1 Motivation

A fundamental objective of geodetic monitoring is the acquisition of geometric object changes under the influence of loads (Heunecke et al. 2013). In particular, the monitoring of supporting structures is of great importance, since the structural members as a whole system of all supporting elements are responsible for the stability of a construction.

Since engineering structures are often systems that are capable of vibration and the predominant part of all load factors has a dynamic character, the focus of corresponding monitoring measurements is set on the collection of temporally variable structural deformations.

Until now, the primary components of such measurement concepts are acceleration sensors, inductive displacement sensors and strain gauges. Although these sensors provide highly accurate data that is optimally adapted to the application, they must be mounted on the measurement object producing an enormous workload. Furthermore, inaccessible areas that do not allow the mounting of these sensors are particularly problematic. In general, the measurement information obtained in this way is only available at discrete object points and cannot be interpreted without appropriate prior knowledge about the supporting structure.

The purpose of this paper is to demonstrate that profile scanners have the potential to solve the discussed problems and to complement existing measurement concepts. Due to the repeated acquisition along a profile, the measurement data possesses both temporal and spatial resolution, which can be ideally combined with the measurement information obtained at discrete points.

In the following section, the measurement system is introduced and the most important parameters are explained. Section 3 shows how the derivation of spatially distributed time series is carried out in the context of a spatio temporal processing scheme. The basic principles are further deepened with practical examples in Section 4 and 5. The focus lies on railway bridges, whereby the examples differ significantly in the occurring deformation signals and bridge characteristics. This shows the potential of the profile scanner for the monitoring of supporting structures and demonstrates the applicability of the developed processing scheme.

2 Measurement system based on a profile scanner

The profile scanner used in this investigation is a phase-based Zoller+Fröhlich Profiler 9012. It is a pure 2D scanner, see Fig. 1. All adapters for using it in the area of monitoring are proprietary developments (tripod and targeting adaptor). Due to the special type of adaptation,
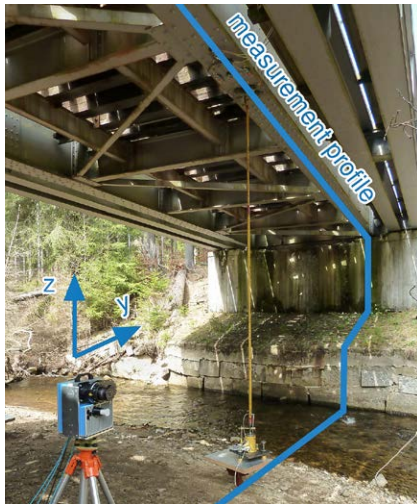
← Fig. 1:
Profile scanner under a railway bridge

→ Fig. 2:
Raw measurement profile with approximately 20,000 points
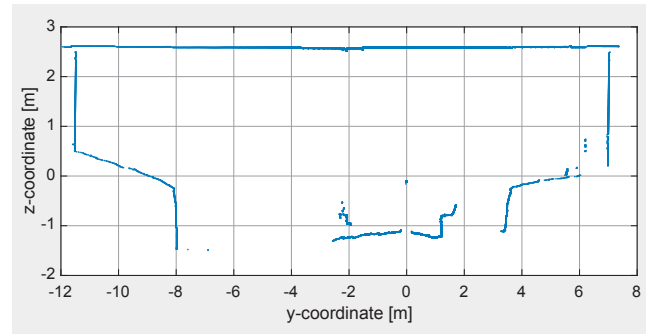
In Fig. 1, a schematic measurement profile and the corresponding coordinate axes are displayed together with the profile scanner. Accordingly, Fig. 2 shows the y/z measurement plane of the profile scanner with approximately 20,000 measurement points in one measurement profile.

both vertical and horizontal measurements are possible. Since the profile scanner is equipped with a GPS receiver, a time stamp can be calculated for each individual point. The manufacturer specifies the maximum measurement distance with 119 m. With a data recording rate of up to 1 million points per second, measuring speeds of 50, 100 or 200 profiles per second are possible (Zoller + Fröhlich 2018).

3 Spatio temporal processing scheme

The profile scanner determines a spatial and temporal component for every measured point, which corresponds to a spatio temporal acquisition of the structural members. However, the original measured values of the profile scanner are not directly usable for the monitoring of supporting structures, as they are not directly accessible and on the other hand not reproducible (Schill 2018).

The measured values (organized in profiles) must therefore be analysed in the context of the structural surface and local conditions. Due to the large number of measurement profiles belonging to a scan, this analysis has to be automated for efficiency reasons. For this purpose, a universally applicable processing scheme has been developed, of which the flowchart is depicted in Fig. 3. The scheme subdivides into three parts:
- the automatic analysis of the measurement profiles,
- the profile wise spatial processing,
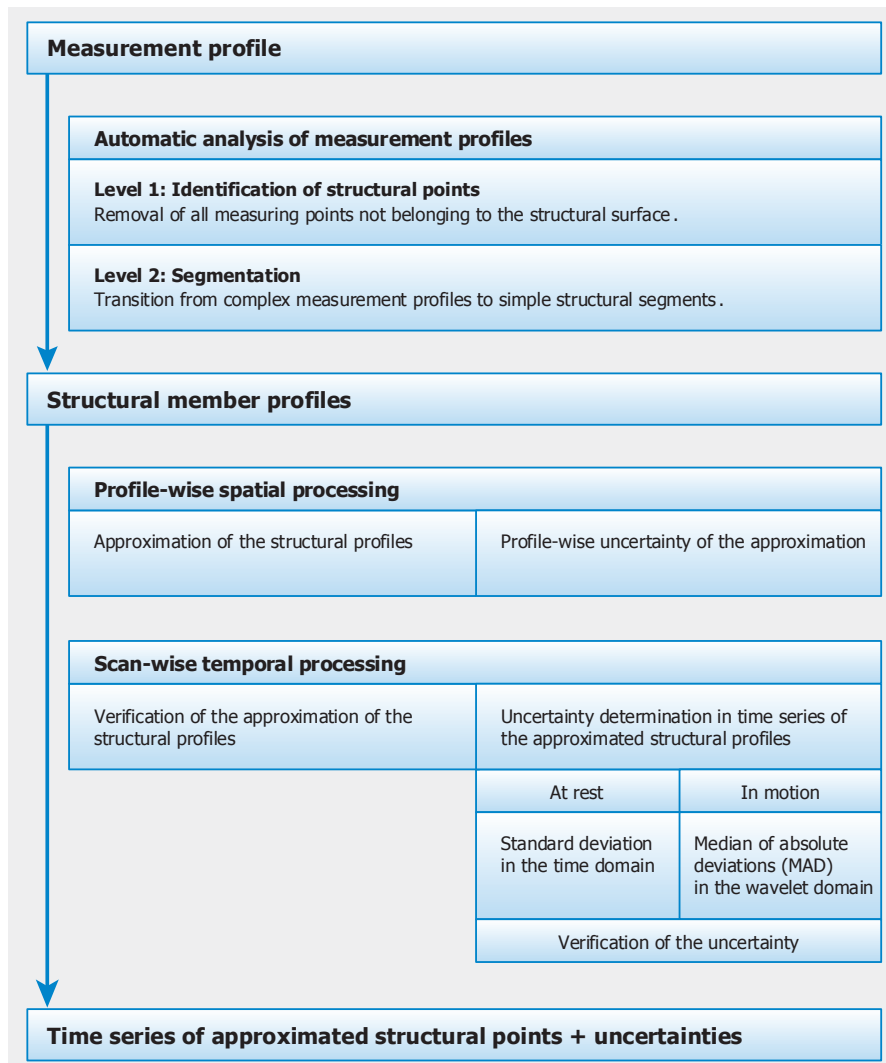- the scan wise temporal processing.

Fig. 3:
Spatio temporal processing scheme

The first step is the automatic analysis of the measurement profiles with the objective to eliminate all measured points not belonging to the structural surface and to segment the complex measurement profiles into simpler segments. This part of the spatio temporal processing scheme is presented in detail in Schill and Eichhorn (2017) and Schill (2018).

Based on those simplified profile segments a profile wise spatial processing can be implemented for example as an approximation with spatial clustering, B-spline functions (De Boor 2001), wavelets (Donoho and Johnstone 1994) or others. Those spatial processing approaches are extensively discussed in Schill (2018).

The choice of the different processing approaches depends heavily on the structure to be examined. In principle, it can be differentiated into two categories: smooth surfaces, as in the investigations of wind turbines in Schill and Eichhorn (2016) or structured object surfaces, which can occur at steel bridge structures (Schill and Eichhorn 2017).

In case of smooth surfaces, the selection of the evaluation strategy is relatively free and depends mainly on the evaluation target, such as the use of continuous functions for the determination of eigenmodes or the spatial clustering for the calculation of eigenfrequencies of the supporting structure.

Independent of the profile wise spatial processing method, after the following scan wise temporal processing, the final results are time series of approximated structural points and corresponding uncertainties. These can be used as a starting point for investigations that optimally capture the deformation behaviour in terms of space and time, thus forming the basis for the monitoring of supporting structures with a profile scanner.

In the following, the application of the spatio temporal processing scheme will be reviewed in detail with two different examples, which vary not only in the before mentioned surface categories, but also in the occurring deformation signals:

■ Example 1: A steel bridge with a heavily structured surface (Section 4) whereas the analysis concentrates on quasi-static deformations.
■ Example 2: A steel bridge with a smooth surface (Section 5) whereas the analysis concentrates on the dynamic deformation component.

4 Example 1: Single-tracked railway bridge over the Flanitz at Klingenbrunn

The examined engineering structure is an over one hundred year old single-tracked railway bridge with a span of just under 20 m. The main beams are designed as solid steel beam and only sit on the two abutments, see Fig. 4. The bridge was subsequently extended by two

Fig. 4: Side view of the single-tracked railway bridge

footpaths, which are connected with the actual bridge only at the abutments.

The deformation monitoring took place during ongoing railway operations. The trains were Regio-shuttle RS1 with an empty weight of approximately 41 tons and a speed at the bridge crossing of approximately 30 km/h. The individual passages are therefore distinguished mainly by the direction of travel and the number of used wagons.

With the profile scanner two different measurement configurations have been recorded which are presented in the following:

■ along the bridge axis on the main beams (Section 4.1),
■ perpendicular to the bridge axis in the middle of the bridge (Section 4.2).

4.1 Analysis of the main beams along the bridge axis

Fig. 5 shows a schematic longitudinal section through the bridge structure along one main beam. Since the two main beams are identical in construction, this figure is representative for both of them. The main beam consist of two full-wall steel beams, which are connected in the middle of the bridge. The two parts of the main beams are additionally stiffened to the middle of the bridge, as seen indicated in Fig. 5 by the increasing thickness.

In the lower diagram of Fig. 6, the result of the automatic analysis of an exemplary measurement profile is shown for the first configuration. According to the
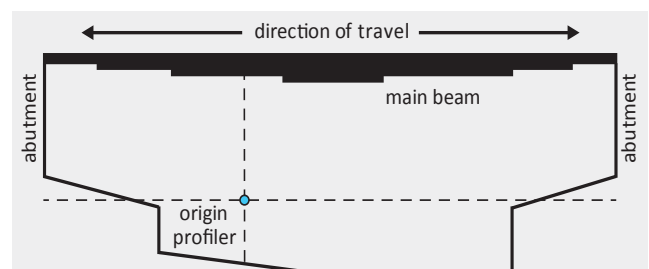
Fig. 5: Schematic longitudinal section through the main beam of the single-tracked railway bridge
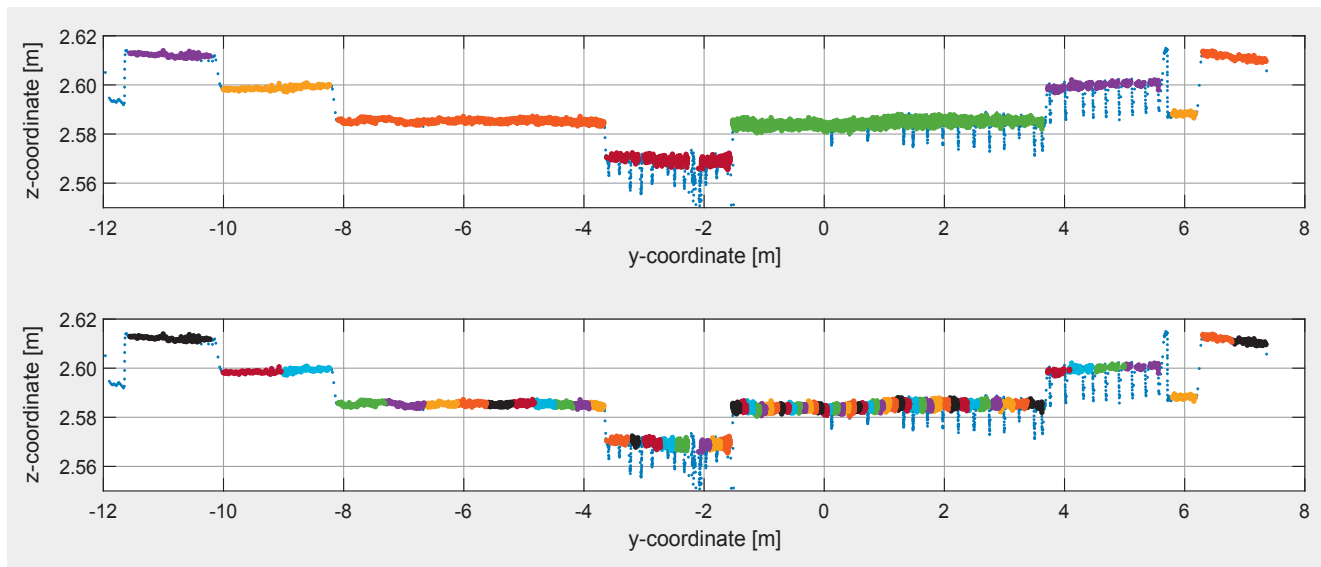
Fig. 6: Upper diagram: Automatic segmented measurement profile along a main beam.
Lower diagram: Spatial clustering based on the automatic segmentation

statements of Section 3, the automatic analysis of the measurement profiles removes erroneous measurements as well as disturbing structural details. Following this, the structure of the surface is segmented based on its details. In the upper diagram of Fig. 6, the measurement points belonging to the resulting structural segments are highlighted in colour from the original profile measurements (in blue). In this case, the surface structure of the main beam leads to a segmentation into eight parts.

The results of the automatic analysis of the measurement profiles are so-called structural segments, which have to be further processed for the spatio temporal determination of the vertical deformation, see Fig. 3. In this case, an approximation with continuous functions such as B-splines or wavelets is not useful, due to the spatially limited segments. Therefore, a spatial clustering is carried out in the following.

The measurement points within such a spatial unit are jointly processed with the aim of producing a derived representative per cluster. With this simple definition, spatial clustering is an almost universally usable processing approach, whose computing power is very low, especially if, as in this example, the cluster representative is formed as the mean value.

The definition of the cluster size is realised using the same angle ranges. Thus, in this case 71 clusters are created, which are highlighted in the lower diagram of Fig. 6 in colour. The spatial extent of the clusters varies between 0.1 m and 1.4 m, but the number of measurement points included in every cluster is almost constant. This offers the advantage that the measurement time for all clusters is about the same and thus the uncertainty due to the sequential measurement has the same magnitude.

By processing the spatially distributed clusters the transition to a spatio temporal representation is created, see Fig. 7. The top chart shows the time series of a cluster representative in the middle of the structure.

In the six diagrams underneath exemplary epochs of the space-time representation are shown on the right side. On the left side, the corresponding position of the train is shown on the bridge. The position, at which the time series shown in the top chart was evaluated, is additionally marked with a blue arrow.

The assignment of the cluster representatives within the epochs of the spatial representation (right side) to the bridge structure in the lower diagram of Fig. 6 is possible based on the consistent colouring of the clusters and their representatives. The temporal mapping of the six spatial representations can be done using the time stamps or the corresponding colouring of the markers in the top chart. In combination with the situational sketches, the top-level diagram is used to illustrate the general sequence of the train crossing.

The load of the wagons is divided between the two bogies, so that the double wagon shown in this example has four load points, the middle two are so close that these can be combined. The following considerations therefore assume three load points with different loads. Since the distance between the bogies of 17 m is almost as large as the span of the main beams with 19.6 m, there is usually only one load point on the bridge at the same time.

Accordingly, the time series of the z-coordinate of the cluster representative in the upper diagram in Fig. 7 shows three local minima. The maximum deflection (middle minimum) occurs when the rear bogie of the first wagon is located on the bridge together with the front bogie of the second wagon (middle load point). The other two local minima are caused by the other bogies of the front or rear wagon.

In the six epochs depicted in Fig. 7, the relative changes of the bridge form are illustrated. This shows that the bending line, as expected, takes on a different shape depending on the position of the bogies of the wagons on the bridge:
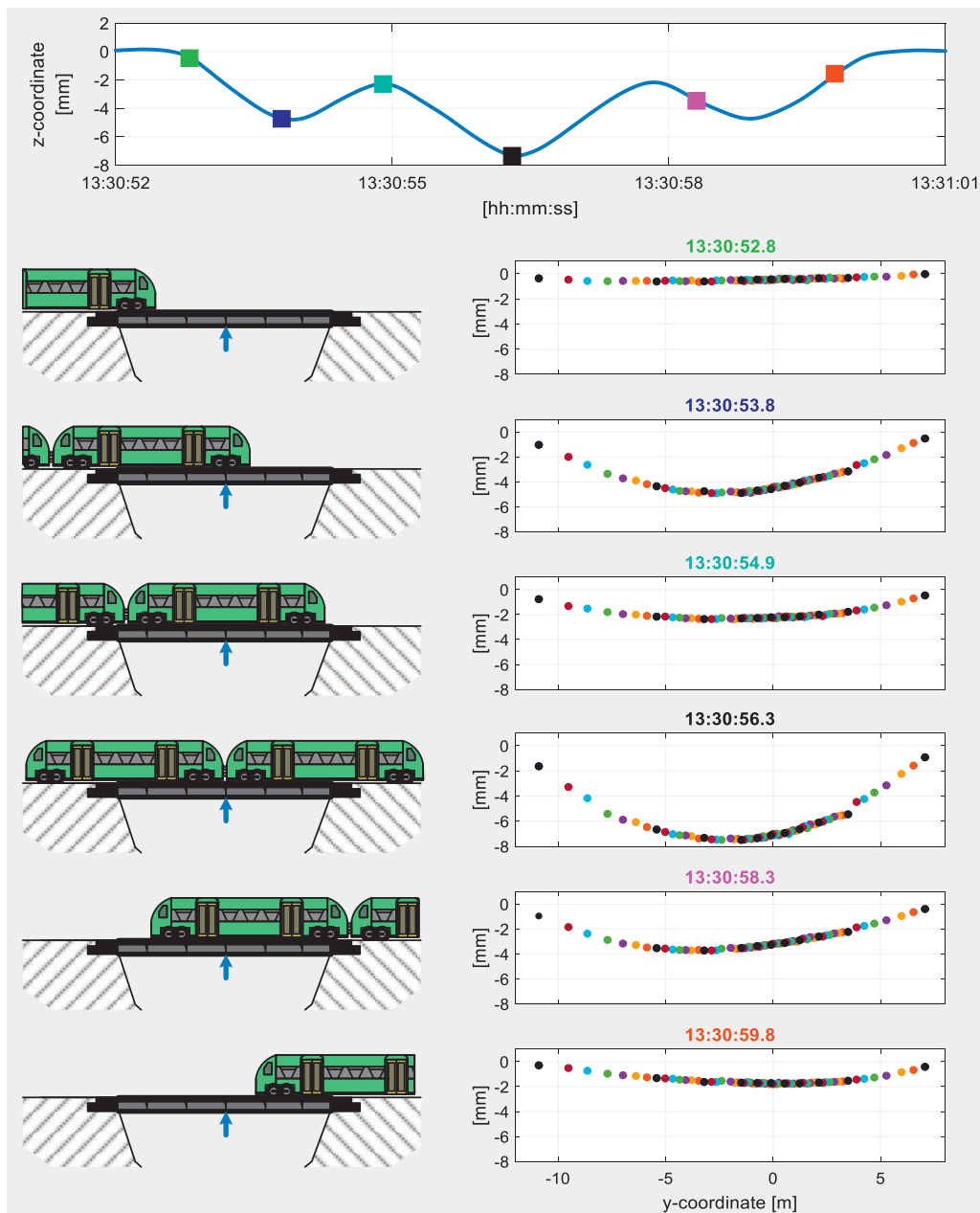
Fig. 7:
Spatio temporal representation of a train crossing with two wagons.
Top graph: Time series of a cluster representative for the classification of the individual epochs of the spatial representation.
The remaining six illustrations correspond to the spatial representation of a defined point in time during the crossing (epochs).

1. The green epoch shows the situation after the front bogie of the first wagon has entered the bridge. The amplitude of the bending line is low and the shape is asymmetric according to the train position.
2. At the time of the blue epoch, the front bogie of the first wagon is located directly in the middle of the bridge, which at this time produces the first local minimum. The shape of the bending line is symmetrical around the centre of the bridge with a maximum amplitude of 5 mm.
3. In the turquoise epoch, the first partial relief of the bridge is shown. The first and second load points are symmetrical to the centre of the bridge at the bridge edges. This also creates a symmetrical bend line characterized in this case by two load points. An almost constant deflection of 2 mm is achieved over a total area of about 9 m.

4. The black epoch shows the maximum load on the bridge produced by the central load point (two bogies). The maximum deflection of nearly 8 mm occurs in the middle of the bridge. However, the load situation corresponds to the blue epoch but with a higher load. In the area of the y-coordinate of 3.5 m, some cluster representatives have a greater deflection than would be expected for a homogeneous bending line. This is the border area of the fourth structural segment from the right, compared to the upper diagram of Fig. 6.
5. The magenta epoch shows a very asymmetrical bending line, since the double-load point just leaves the bridge; the last bogie is not yet in the middle of the bridge.
6. The time of the red epoch shows the situation just before the last bogie leaves the bridge. The shape of the bending line is similar to a mirrored version of the green epoch.

The spatio temporal processing scheme allows the acquisition of the entire surface structure within a profile. Therefore, it is possible to measure the complete bending line directly, and to detect deviant behaviour of individual profile segments, as seen exemplary in the black epoch in Fig. 7.

In comparison, this is not practicable with conventional sensors for the monitoring of bridges, because the density of the discrete measurement points is usually much sparser. Therefore, the choice of the discrete measurement positions has to be planned based on appropriate prior knowledge about the supporting structure or on the theoretical deformation behaviour.

The usage of profile scanning has the advantage that there is no need for such an extensive measurement planning. On the contrary, it offers high flexibility combined with low planning expenses.

4.2 Analysis of the main beams perpendicular to the bridge axis

In addition to the evaluation of the vertical component shown in the previous analyses, the horizontal deformation of the bridge can be recorded in particular with the measurements of configuration 2. The following section therefore concentrates on the evaluation of this configuration, which was measured perpendicular to the main bridge axis. The focus lies on the simultaneous recording of the horizontal deformation of both main beams.

Due to the fact that the bridge is located in a curve of the railway track, in addition to the vertical deformation there exists also a horizontal deformation. This is caused by the combination of the centrifugal force due to the position in a curve and the force because of the sine run of the train (Liu 2011).

To determine the horizontal deformation, a modified automatic analysis of the measurement profiles has to be performed, wherein the analysis focuses on the y-coordinate values. Based on the resulting segmentation, a spatial clustering was executed, the result of which is shown in the upper diagram in Fig. 8. The cluster definition is based on a constant angle range, so that all clusters contain approximately the same number of measurement points.

For the determination of the horizontal deformation of the two main beams, the blue cluster is selected at the main beam 1 and the red cluster at the main beam 2 as representative examples. Both clusters have a vertical extension of approximately 0.15 m and include approximately 80 points.

The lower diagrams of Fig. 8 show the time series of the representatives of the blue and red cluster. Both time series are divided into three parts: before the crossing, during the crossing and after the crossing, which are visually separated from each other by black lines. The uncertainty for the y-coordinate of the two cluster representatives can be determined from the cut-outs before and after the crossing (without load) in the time domain. For the blue time series the standard deviation results in approximately 0.13 mm and the standard deviation of the red time series results in approximately 0.11 mm.

Using these results, the cut-out during the crossing is wavelet denoised and the result is superimposed in black on the actual deformation signal. In both time series, the
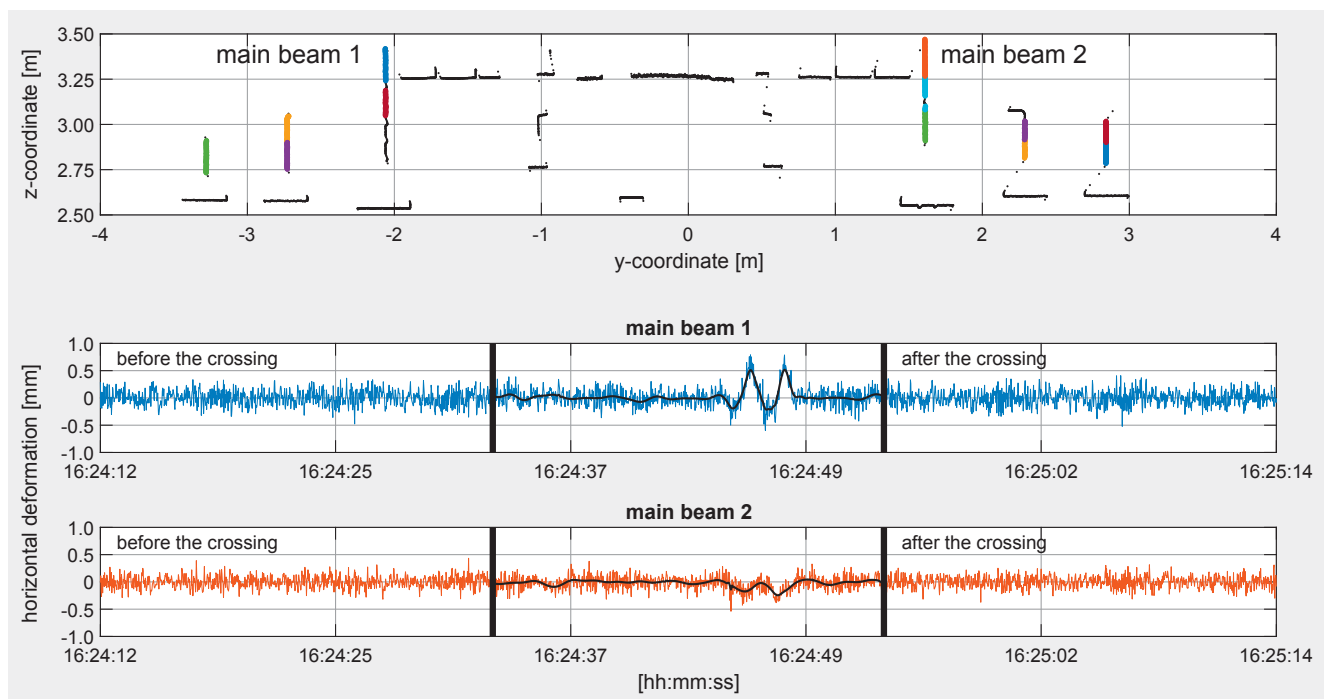

Fig. 8: Upper diagram: Spatial clustering based on the automatic segmented profile for configuration 2.
Lower diagram: Time series of the representatives of the blue and red cluster

horizontal deformations induced by the forces from the bogies of the train can be verified. The main beam 1 (outside of the curve) has a maximum horizontal deformation of over 0.5 mm at the crossing of the bogies. For the main beam 2, the magnitude of the horizontal deformation is just above the noise level. This shows that due to the position in the curve most of the horizontal load rests on the outer track.

The possibility of a combined analysis of the vertical (Section 4.1) and horizontal deformation of a supporting structure, provides the possibility to gain extensive information about the structural behaviour in order to improve the planning and execution of measurement campaigns. For example, the analysis to what extent the lateral deformation of the bridge influences the results of other sensors measuring the vertical deformation, see Becker at al. (2016).

5 Example 2: Trough bridge over the Aller

The second monitored engineering structure is a newly built railway bridge over the Aller near Verden (Niedersachsen). The bridge is 380 m long, consisting of seven bridge spans and was executed as a joint less steel bridge. The maximum route speed is 160 km/h. All measurements took place at the eastern main beam of the bridge in longitudinal direction. The measured bridge span has a length of approximately 50 m, see Fig. 9. In contrast to the single-tracked railway bridge from Section 4, the surface of the main beam has no structuring, so that the automatic analysis of the measurement profiles only creates one profile segment.

For this reason, all spatial processing methods presented in Section 3 are suitable for further analyses. Fig. 10 depicts the results of the spatial clustering and the B-spline approximation for a single measurement profile on the eastern main beam between two supports.

The profile points are divided into 100 spatial clusters and are coloured accordingly. The expansion of the spatial clusters is again chosen in such a way that all cluster contain approximately the same number of profile measurement points (approximately 90 points each), which varies the cluster extent between 0.1 m and 4 m. In addition, a B-spline approximation is superimposed

Fig. 9: Trough bridge over the Aller

on the measurement points in black. For the theoretical background, see e.g. Neuner et al. (2013), Bureick et al. (2016) and Schill (2018).

In order to compare the results of the two profile wise spatial processing methods, the same positions on the supporting structure were evaluated. These positions are specified in this case by the representatives of the 100 clusters and were evaluated with the B-spline approximation. Therefore, a total number of 100 time series distributed over the entire structure are available.

In the upper diagram in Fig. 11, the time series of the z-coordinates for both processing methods at one position (y-coordinate –10.39 m) are depicted. It is a 50-second section of the crossing of a freight train, which was recorded with 50 Hz and contains therefore 2,500 measurement profiles. The lower diagram shows the differences between the two processing methods. These differences do not contain any systematic effects and are mainly caused by the slightly larger noise level of the spatial clustering. Based on that fact, the results of the profile wise B-spline approximation will be used in the following.

The time series in the upper diagram of Fig. 11 consists primary of a low-frequency signal component due to the load of the train and a superpositioned high-frequency signal component due to the dynamic excitation of the bogies of the train. In the following, these two parts are called the quasi-static and the dynamic signal component of the time series.

With the use of the multiresolution analysis (MRA) of the discrete wavelet transform, not only noise can be
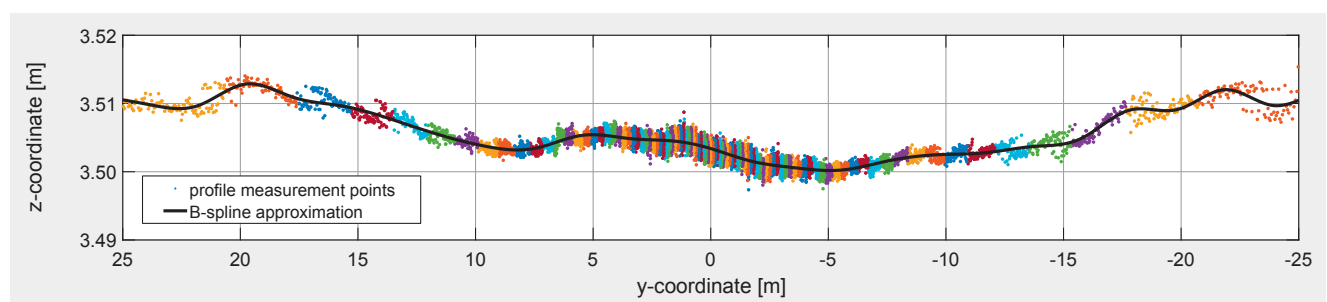

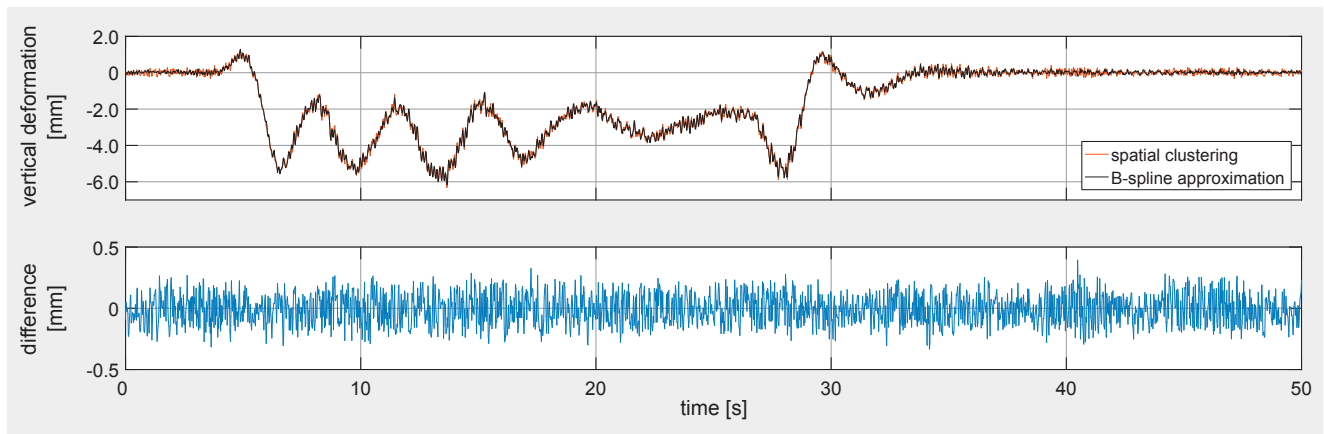Fig. 10: Results of two processing methods: spatial clustering (coloured) and B–spline approximation (black)

Fig. 11: Time series of the z–coordinates of both processing methods at the y–coordinate –10.39 m and their differences
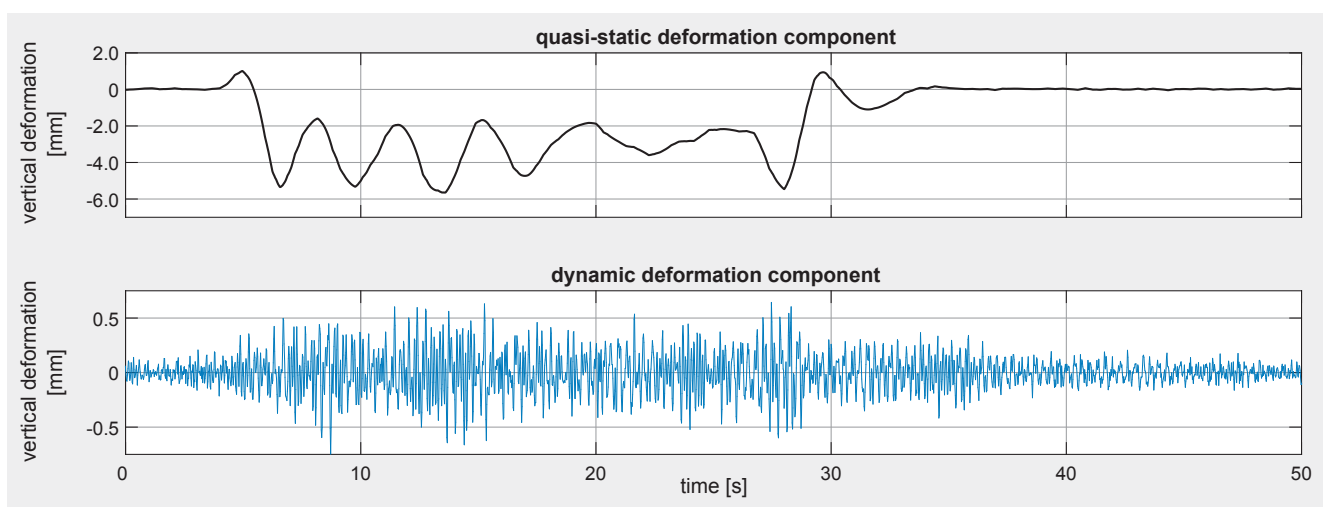

Fig. 12: Separation of the dynamic and quasi–static deformation component of the sample time series from Fig. 11

eliminated, but it is also possible to separate frequency ranges. The MRA decomposes the signal into individual frequency bands, see e. g. Bäni (2005) and Percival and Walden (2000). With the wavelet synthesis the desired signal components can be reconstructed and thus, the transition from the total deformation to the dynamic deformation component can be realized, see Fig. 12. In the upper diagram, the black line shows the quasi-static deformation component determined by means of wavelet decomposition/synthesis. The time series of the dynamic deformation component is shown in the lower diagram in blue.

Based on the separation of the quasi-static from the dynamic deformation component, two selected positions on the structural member are analysed in the following. These are a position in the middle of the field (y-coordinate: –0.05 m, yellow) and approximately the quarter point (y-coordinate: –10.39 m, purple). These two positions are highlighted in the top chart in Fig. 13 with coloured dots and in Fig. 14 with coloured lines. The choice of these positions is based on the theoretical eigenmodes of a simple beam (Gross et al. 2018), shown in Fig. 14. This simple model can also be a good approxi-

mation for bridges. While in the middle of the beam the first eigenmode has its maximum, the second eigenmode has a zero pass. In the quarter point, however, the second eigenmode has its maximum, while the amplitude of the first eigenmode decreases.

In the lower diagrams of Fig. 13, the dynamic deformation components of the time series are shown on the left side and the corresponding amplitude spectra on the right side. For the two positions on the structure, three frequency ranges can be identified in the amplitude spectra, in which amplitudes occur above the noise level: approximately at 2 to 3 Hz, at 5 Hz and at 8 Hz.

The so far considered time series include the train crossing, as well as areas in which the supporting structure is at rest and the free decay process of the structure. Therefore, it is not possible to make a valid statement about the association of those frequency ranges to the natural frequencies. In principle, it can only be seen that certain frequencies within the time series have occurred at least temporarily.

To avoid this restriction we will concentrate on a shorter part of the time series: the free decay process after the train left the monitored bridge span. Due to the
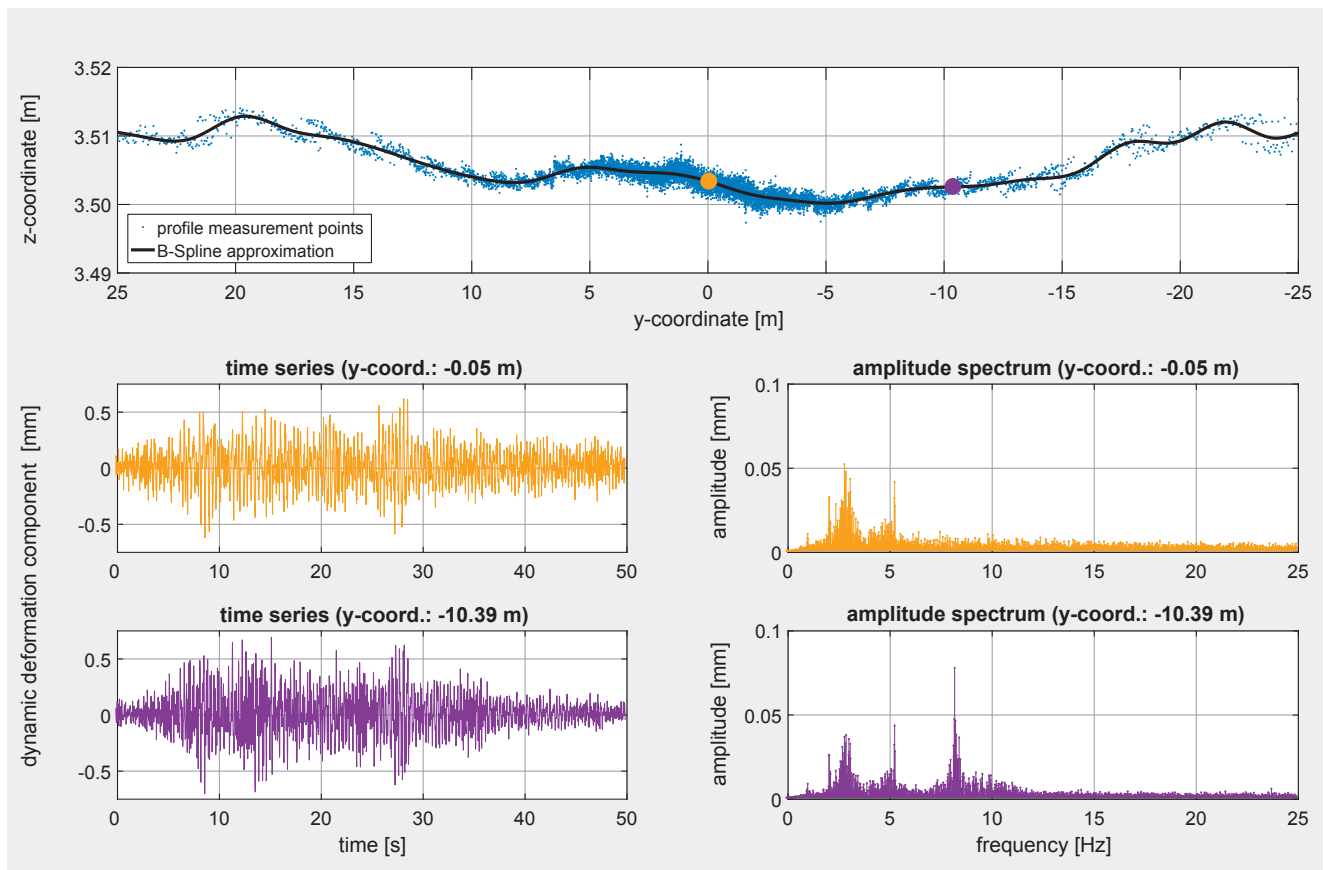
Fig. 13: Dynamic deformation component in the time- and frequency domain at two discrete points of the bridge span

high spatial resolution of the profile scanner, we can simultaneously widen our view in the context of spatial resolution.

The two-position representation in Fig. 13 corresponds to the traditional analysis of conventional discrete sensors used for the monitoring of bridges. However, the almost space-continuous detection of the structural surface with the profile scanner can be used to view the entire bridge span in detail, maintaining a temporal resolution of 20 ms, for a corresponding waterfall representation see Fig. 15. On the x-axis, the position on the structure is shown, on the y-axis the frequency range (limited to the relevant area up to 12 Hz) and on the z-axis, the magnitude of the amplitudes is plotted. Thus, the free decay process is represented in the frequency domain for the entire bridge span.

In contrast to Fig. 13, significant amplitudes occur in Fig. 15 only at the frequency ranges of 3.1 and 8.3 Hz. The previously occurring amplitudes at 5 Hz and the sec-

ondary maxima in the frequency range around 3 Hz are no longer existing.

Hence, it can be concluded that 3.1 Hz is the first natural frequency (eigenfrequency) and 8.3 Hz is the second natural frequency. Since the associated distribution of the amplitude maxima corresponds mostly to the theory as seen in Fig. 14.

This is further confirmed by the phase position of the occurring frequencies, which is constant for 3.1 Hz (first natural frequency) over the entire structure, while the phase position for 8.3 Hz (second natural frequency) is symmetrically to the middle of the bridge, but with inverse sign.

However, the amplitudes of the likely second eigenmode increase on both sides until the end of the measured bridge span. According to the theory from Fig. 14, there should be a decrease in amplitude beginning at the quarter point until the support. This difference between the theory and the profile scanner measurements is likely caused by the too simple model, which does not take into account the real support conditions and the fact that the bridge consists of seven bridge spans.

In conclusion, those differences can only be evaluated with the high spatial resolution of the profile scanner. In most cases, only measurements at predefined points (according to the theory) are available, like the graphs depicted in Fig. 13.
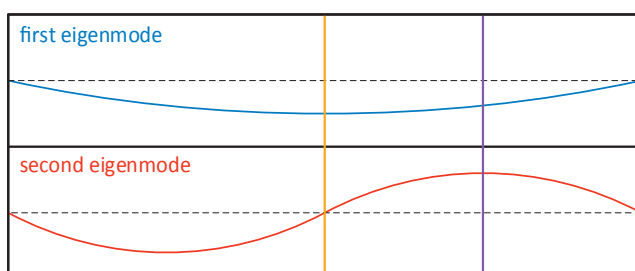

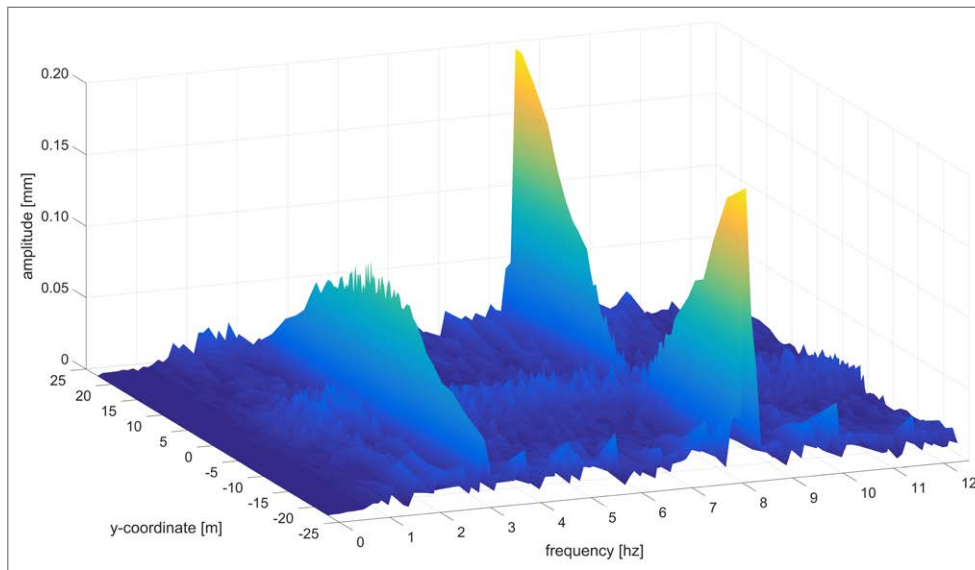Fig. 14: Theoretical eigenmodes of a beam

Fig. 15:
Amplitude spectra of the dynamic deformation component for the free decay process of the monitored bridge span

6 Conclusions

The two examples demonstrate that a non-contact measurement system like a profile scanner can capture temporally variable structural deformations more efficiently and in a much higher spatial resolution than typically used sensors for the deformation monitoring of supporting structures. Furthermore, it is possible, with the presented measurement and evaluation methodology, to reach uncertainties of nearly the same scale as generated with conventional discrete measurement sensors.

Due to the high spatial and temporal resolution, large amounts of data are recorded. For practical use, this implies that the automatically collected data needs a largely automated processing and quality assessment.

With the spatio temporal processed data basis it is possible to derive deformation measurements at nearly any desired position within a supporting structure profile (post mission). Therefore, the dependence on prior knowledge about the structure or on the theoretical deformation behaviour is greatly reduced. That applies to the measurement planning as well as the analysis of the deformation behaviour.

The adaptable spatial resolution furthermore enables the detection of model disruptions or deviant behaviour of parts of the supporting structure. Thus, it is possible to verify structure models and to improve their predictive quality accordingly.

References

Bäni, W. (2005): Wavelets: Eine Einführung für Ingenieure. Oldenbourg Verlag, ISBN: 9783486594003.

Becker, M., Traiser, B., Schill, F., Schneider, J., Firus, A. (2016): Messung und Identifikation dynamischer Strukturparameter mittels terrestrischer Mikrowelleninterferometrie. Messen im Bauwesen.

Bureick, J., Alkhatib, H, Neumann, I. (2016): Robust Spatial Approximation of Laser Scanner Point Clouds by Means of Free-form Curve Approaches in Deformation Analysis. Journal of Applied Geodesy. Vol. 10, Issue 1, pp. 27–35.

De Boor, C. (2001): A practical guide to splines. Applied mathematical sciences, Springer-Verlag, ISBN: 9780387953663.

Donoho, D., Johnstone, I. (1994): Ideal spatial adaptation by wavelet shrinkage. Biometrika 81.3, pp. 425–455.

Gross, D., Hauger, W., Wriggers, P. (2018): Technische Mechanik 4: Hydromechanik, Elemente der Höheren Mechanik, Numerische Methoden. Springer-Verlag, ISBN: 9783662556948.

Heunecke, O., Kuhlmann, H. Welsch, W., Eichhorn, A., Neuner, H. (2013): Handbuch Ingenieurgeodäsie – Auswertung geodätischer Überwachungsmessungen. Springer-Verlag, ISBN: 9783879074679.

Liu, J. (2011): Einfluss der Schienenbefestigungskomponenten auf das laterale Verformungs- und Lastverteilungsverhalten der Schiene. Dissertation, Technische Universität München, München.

Neuner, H., Schmitt, C., Neumann, I: (2013): Modelling of terrestrial laser-scanning profile measurements with B Splines. In: Proc. of 2nd Joint international Symposium on Deformation Monitoring (JISDM). 09.–12.09.2013 in Nottingham (UK).

Percival, D., Walden, A. (2000): Wavelet Methods for Time Series Analysis, Cambridge Series in Statistical and Probabilistic Mathematics. Cambridge University Press, ISBN: 9780521640688

Schill, F., Eichhorn, A. (2016): Investigations of low- and high-frequency movements of wind power plants using a profile laser scanner. In: Proc. of 3rd Joint International Symposium on Deformation Monitoring (JISDM). 30.03.–01.04.2016 in Vienna (Austria).

Schill, F., Eichhorn, A. (2017): Automatische Segmentierung von Profilscannermessungen am Beispiel von Brückenbauwerken. In: Ingenieurvermessung 17 – Beiträge zum 18. Int. Ingenieurvermessungskurs. Lienhart W (eds). 25.–29.04.2017 in Graz (Austria), pp. 389–401.

Schill, F. (2018): Überwachung von Tragwerken mit Profilscannern. Deutsche Geodätische Kommission (DGK), Reihe C, Nr. 820, identical with TUprints – E-Publishing-Service der TU Darmstadt URN: urn:nbn:de:tuda-tuprints-72679.   http://tuprints.ulb.tu-darmstadt.de/7267.

Zoller + Fröhlich (2018): Z+F PROFILER® 9012 Datasheet. www.zf-laser.com/fileadmin/editor/Datenblaetter/Z_F_PROFILER_9012_Datenblatt_D_final_kompr.pdf, visited at 10.12.2018.

Contact
Florian Schill | Andreas Eichhorn
TU Darmstadt, Institut für Geodäsie, Fachgebiet Geodätische Messsysteme und Sensorik
Franziska-Braun-Straße 7, 64287 Darmstadt
schill@geod.tu-darmstadt.de | eichhorn@geod.tu-darmstadt.de

This article also is digitally available under www.geodaesie.info.